Title

Redox-Controlled Reactivity at Boron: Parallels to Frustrated Lewis/Radical Pair Chemistry

Journal

Inorganic Chemistry, 59(14)

ISSN

0020-1669

Authors

Wong, Anthony
Chu, Jiaxiang
Wu, Guang
et al.

Publication Date

2020-07-20

DOI

10.1021/acs.inorgchem.0c01464

Peer reviewed

Inorganic Chemistry

pubs.acs.org/IC Article

Redox-Controlled Reactivity at Boron: Parallels to Frustrated Lewis/Radical Pair Chemistry

Anthony Wong,[⊥] Jiaxiang Chu,[⊥] Guang Wu, Joshua Telser, Roman Dobrovetsky, and Gabriel Ménard*

Cite This: https://dx.doi.org/10.1021/acs.inorgchem.0c01464 Read Online

ACCESS | Metrics & More | Article Recommendations | Supporting Information

ABSTRACT: We report the synthesis of new Lewis-acidic boranes tethered to redox-active vanadium centers, $(Ph_2N)_3V(\mu\text{-}N)B(C_6F_5)_2$ (**1a**) and $(N(CH_2CH_2N(C_6F_5))_3)V(\mu\text{-}N)B(C_6F_5)_2$ (**1b**). Redox control of the $V^{IV/V}$ couple resulted in switchable borane versus "hidden" boron radical reactivity, mimicking frustrated Lewis versus frustrated radical pair (FLP/FRP) chemistry, respectively. Whereas heterolytic FLP-type addition reactions were observed with the V^{V} complex (**1b**) in the presence of a bulky phosphine, homolytic peroxide, or Sn−hydride, bond cleavage reactions were observed with the V^{IV} complex, $[CoCp_2^*][(N(CH_2CH_2N(C_6F_5))_3)V(\mu\text{-}N)B(C_6F_5)_2]$ (**3b**), indicative of boron radical anion character. The extent of radical character was probed by spectroscopic and computational means. Together, these results demonstrate that control of the $V^{IV/V}$ oxidation states allows these compounds to access reactivity observed in both FLP and FRP chemistry.

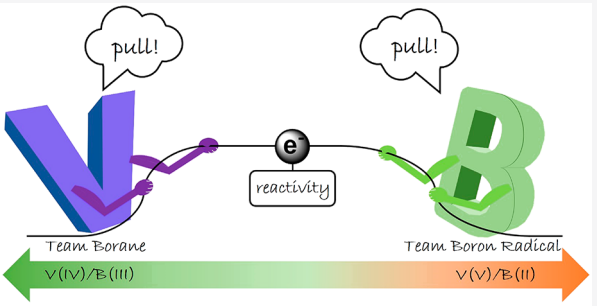

A radical "tug-of-war" between V and B enables bond activation mimicking frustrated Lewis or radical pair chemistry through $V^{IV/V}$ redox control.

INTRODUCTION

The past two decades have seen a dramatic increase in reported main-group-mediated bond activation chemistry.[1−5] Frustrated Lewis pair (FLP) chemistry has been a significant contributor to this increase, stimulating intrigue spanning multiple fields while unlocking new applications in main-group chemistry.[6−8] Whereas FLPs can activate an ever-expanding repertoire of small molecules (H_2, CO_2, N_2O, CO, etc.) and bonds (C−H, alkenes, alkynes, etc.), the commonly accepted mechanism features initial element−element bond polarization within the pocket of an "encounter complex" generated by the close interaction of the Lewis pair, followed by a two-electron, concerted heterolytic bond activation step.[9−11] However, recent work has uncovered a possible homolytic pathway mediated by transient ionic phosphine/borane frustrated *radical* pairs (FRPs) generated by single-electron transfer (SET) (Scheme 1).[12−18] The existence of these FRPs was supported by combined spectroscopic (i.e., EPR) and reactivity studies, with the latter focusing on the unique chemistry of the generated boron radical anion, such as homolytic peroxide or Sn−hydride bond cleavage, similar to related reports using isolated boron radical species.[19−23]

Our group has been exploring new reactivity at main-group centers by tethering these to redox-active metal centers, such as V or Fe.[24−28] In a recent contribution, we uncovered how a typically unreactive P^{V}═O bond tethered to a neighboring V^{V} center in the complexes $(Ph_2N)_3V$═N−$P(O)Ar_2$ (Ar = Ph, C_6F_5) can engage in H atom (H·) or silyl group (Me_3Si·) transfer chemistry, resulting in the proposed protonation or

Scheme 1[a]

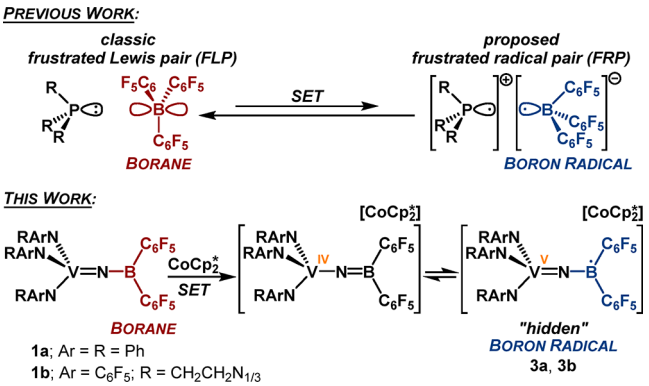

[a]Classical FLP containing a bulky phosphine with a bulky borane and proposed FRP generated by SET containing a boron radical anion (top). This work highlights the switchable reactivity from a borane to a "hidden" boron radical anion by redox control (bottom).

Received: May 20, 2020

https://dx.doi.org/10.1021/acs.inorgchem.0c01464
Inorg. Chem. XXXX, XXX, XXX−XXX

isolated silylation of the P^V=O bond, respectively, with the concurrent reduction of V^V to V^{IV}.[28] Similar reactivity was not observed in related all-main-group model compounds (ex. Ph_3PO), highlighting the cooperative role of the metal center in enabling new main-group-centered reactivity. In this Article, we targeted V-tethered Lewis-acidic B complexes (**1a**,**b**), which, by control of the V redox state, exhibited either FLP chemistry in the borane (V^V) state or reactivity analogous to the B partner in FRPs when in the boron radical anion (V^{IV}) state (Scheme 1). The borane engaged in heterolytic bond activation chemistry, whereas the "hidden" boron radical anion reacted homolytically. This complementary reactivity profile draws significant parallels to the alternating reactivity found in FLPs versus FRPs.

RESULTS AND DISCUSSION

The synthesis of our initial target complexes (**1a**,**b**) followed an analogous approach to our previously reported $(Ph_2N)_3V$=N−P(O)Ar_2 ("VNP") complexes[28] and involved salt metathesis between $ClB(C_6F_5)_2$[29] and the known precursor, $(Ph_2N)_3V(\mu\text{-}N)Li(THF)_3$,[30] or the new tren-based precursor, $N(CH_2CH_2N(C_6F_5))_3V(\mu\text{-}N)Li(THF)_3$, to yield complexes **1a** and **1b**, respectively (Scheme 1). The tren-based precursor was prepared in three steps by initial acid−base metalation using the known protonated ligand[31] and $V(NTMS_2)_3$,[32] followed by V^V imine formation with $TMSN_3$ and desilylation using *i*PrNHLi (see the Experimental Section).[30] Single crystals suitable for X-ray diffraction (XRD) studies were grown for both **1a** and **1b**. The solid-state structures for **1a** (Figure 1) and **1b** (Figure S70) revealed expected trigonal

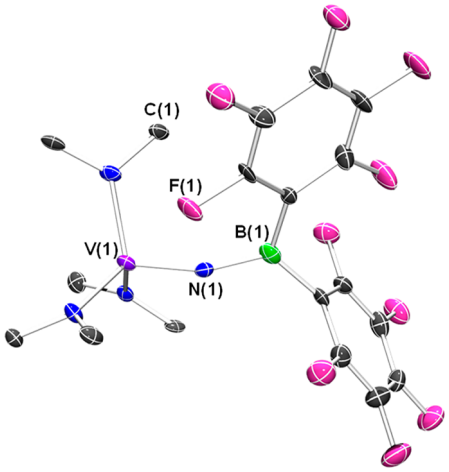

Figure 1. Solid-state molecular structure of **1a**. C_6H_5 groups (except for ipso carbons) and all hydrogen atoms are omitted for clarity.

planar B centers with observed B−N (1.421(11) Å (**1a**); 1.428(6) Å (**1b**)) and neighboring V=N (1.670(6) Å (**1a**), 1.703(4) Å (**1b**)) bond lengths similar to previous reports.[28,33] The resulting V=N−B angles differed substantially from one another (161.1(6)° (**1a**), 170.0(3)° (**1b**)). with both deviating more from linearity than in the reported VNP case (175.9(7)°).[28] The analysis of the products by multinuclear nuclear magnetic resonance (NMR) spectroscopy revealed expected broad ^{11}B resonances (31.8 ppm (**1a**), 30.1 ppm (**1b**)) consistent with three-coordinate B centers.[33,34] Whereas the ^{51}V resonance for **1a** (120 ppm) was similar to that of the VNP analog (117 ppm),[28] the resonance for **1b** (−79 ppm) was significantly shifted, likely due to the higher coordination number at V.[35] Whereas borane-substituted early metal imido complexes are known,[36−42] to the best of our knowledge, these represent the first examples incorporating boranes with strongly electron-withdrawing substituents.

We observed that **1a** was unstable and readily decomposed within hours in solution at room temperature, as observed by multinuclear NMR spectroscopy (Figures S50−S52). One of the decomposition products, $Ph_2NB(C_6F_5)_2$, was identified through independent synthesis, whereas the V-containing decomposition product remains unknown (Figures S46−S49). We attributed this decomposition pathway to the close proximity of the Lewis-acidic B center to the labile Lewis-basic Ph_2N^- groups. Dissolving **1a** in coordinating solvents (tetrahydrofuran (THF), MeCN) led to adduct formation and slower decomposition, as observed by NMR spectroscopy (Figures S62 and S63). The coordinating solvent molecules could be readily removed *in vacuo*, indicating reduced Lewis acidity at B in **1a** compared with $B(C_6F_5)_3$,[43] the Lewis acid of choice in FLP chemistry.[6−8] Not surprisingly, the decomposition pathway observed in **1a** was not observed in **1b** due to the chelating tren ligand.

We next investigated whether **1b** could act as an effective Lewis acid partner in FLP chemistry. Whereas combinations of **1b** with bulky phosphines ($PtBu_3$, $PMes_3$, Mes = 2,4,6-trimethylphenyl) led to no changes in the NMR spectra compared with isolated Lewis partners—the hallmark of FLP formation—no reaction with small molecules (H_2, CO_2) was observed. Whereas the reduced Lewis acidity at B may be partially responsible, we believe that the extreme steric crowding at B due to the flanking tren aryl groups, as observed in the space-filling depiction of the solid-state structure (Figure S71), likely plays a bigger role. Therefore, we attempted to use a more donating, "longer" *para*-benzoquinone molecule, previously used in FLP chemistry.[12] Mixing equimolar amounts of **1b**, $PMes_3$, and tetrafluoro-1,4-benzoquinone in dichloromethane (DCM) resulted in the immediate formation of a new product (Figure 2a), as observed by NMR spectroscopy. Single crystals suitable for XRD studies were obtained and confirmed the formation of compound **2-F$_4$** (Figure 2b), featuring the FLP addition across the benzoquinone moiety. We note that the analogous reaction with unsubstituted benzoquinone to yield the product **2-H$_4$** was also obtained, although it was only characterized crystallographically (Figure S72). Lastly, we note that the mechanism of activation here is unlikely to proceed through an SET mechanism, sometimes proposed with $PMes_3$,[12,44] due to the inability of **1b** to oxidize $PMes_3$ to any appreciable extent (*vide infra*).[45]

Whereas the B centers in **1a**,**b** are Lewis-acidic, we next probed if boron radical character could be accessed by redox-control. Because of the instability of **1a**, we only investigated the electrochemical profile of **1b** by cyclic voltammetry (CV) in DCM. A clean, reversible redox event at $E_{1/2}$ = −1.10 V, referenced to the ferrocene/ferrocenium (Fc/Fc^+) redox couple (Figure 3a), was observed and attributed to the $V^{IV/V}$ redox couple. This reduced complex was chemically isolated by treating **1b** with decamethylcobaltocene, $CoCp_2^*$ ($E_{1/2}$ = −1.94 V in DCM).[46] We note here that **1a** could also be reduced using this method, albeit in lower isolated yields due to its instability. The reduced products, **3a** and **3b** (Scheme 1), were slowly crystallized, and low-resolution solid-state structures were obtained by XRD studies (Figures S73 and S74). We

https://dx.doi.org/10.1021/acs.inorgchem.0c01464
Inorg. Chem. XXXX, XXX, XXX−XXX

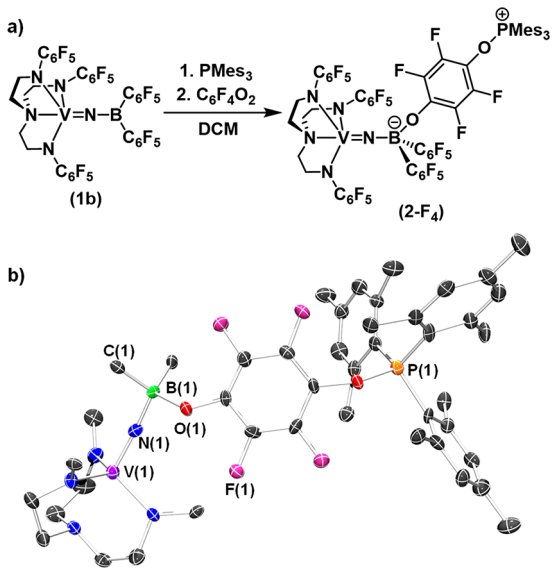

Figure 2. (a) FLP addition of **1b**/$PMes_3$ to tetrafluoro-1,4-benzoquinone to produce **2-F$_4$**. (b) Solid-state molecular structure of **2-F$_4$**. C_6F_5 groups (except for ipso carbons), hydrogen atoms, and cocrystallized solvent molecules are omitted for clarity.

note that a high-resolution structure was obtained by generating a cobaltocene ($CoCp_2$) analog of **3b**, termed **3b′** (Figure S75). Both **3a** and **3b′** contained significantly elongated V−N(B) bonds (1.885(8) Å (**3a**), 1.776(4) Å (**3b′**)) and shortened B−N bonds (1.368(14) Å (**3a**),1.354(7) Å (**3b′**)) relative to **1a**,**b** (*vide supra*). The resulting V−N−B angle in **3a** was significantly more bent (139.2(9)°) relative to **1a** (161.1(6)°), similar to the observed trend upon the reduction of the VNP analog[28] and suggesting a simplified single- and double-bonded structure (V−N═B) with the reduction event mostly localized at V. In stark contrast, the V−N−B linkage in **3b′** (173.9(4)°) changed only slightly relative to **1b** (170.0(3)°), which may suggest a more delocalized V⋯N⋯B π framework enforced by the flanking tren aryl groups.

Compounds **3a** and **3b**/**3b′** were further analyzed by X-band EPR spectroscopy. The room-temperature spectrum of **3a** revealed an expected isotropic eight-line hyperfine splitting pattern due to the coupling of the d^1 electron to the ^{51}V center (I = 7/2) (Figure S64). Anisotropic spectra were observed at 100 K for all species (Figure 3b, Figures S65−S67) and were similar to our reported VNP system.[28] The lack of resolved hyperfine coupling to ^{11}B suggests little to no delocalization of the d^1 electron along the V−N−B framework.[47] However, simulating the data in the absence of ^{11}B coupling led to sharper line widths and a poorer fit with the experimental data (Figure S66), which may suggest some delocalization to B and consequently N. The expected coupling to ^{11}B may simply be too weak to be observable by EPR spectroscopy.[48−50] Therefore, we turned to DFT studies to further probe this. Calculations performed on the anion of **3b** revealed some degree of delocalization of the single electron to the B center along the V⋯N⋯B π framework, suggesting the presence of a "hidden" boron radical (Figure 3c). In particular, whereas the majority of the spin density resided on V (82%), in agreement with our EPR data, the spin density on B (13%) was found to be non-negligible.[51] As previously noted, whereas several early metal borylimido complexes have been prepared,[36−42] to the best of our knowledge, their redox properties have not been investigated as they have been here.

Similar to **1a**, compound **3a** was found to be very unstable in noncoordinating solvents. Whereas we attributed the migration of Ph_2N^- to B as being responsible for the decomposition of **1a**, the decomposition of **3a** was noticeably different. Monitoring a solution of paramagnetic **3a** in a mixture of benzene-d_6 and bromobenzene-d_5 by multinuclear NMR spectroscopy at room temperature revealed the appearance of a main diamagnetic decomposition product (Figures S53−S55), with resonances in the ^{19}F (−127, −164, −167 ppm) and ^{11}B (−2.0 ppm) spectra, consistent with the formation of a four-coordinate boron center.[43] Interestingly, the ^{1}H NMR spectrum revealed a major species having inequivalent

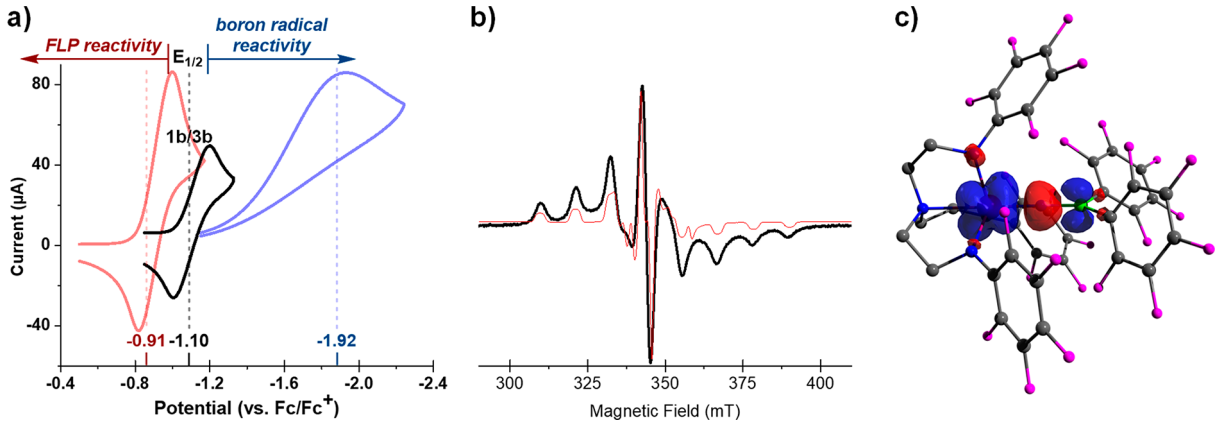

Figure 3. (a) Cyclic voltammograms (250 mV/s) of **1b** (black) (3.0 mM), 2,4,6-*t*$Bu_3C_6H_2O$· (red) (3.0 mM), and dibenzoyl peroxide (PhC(O)OOC(O)Ph) (blue) (3.0 mM) in DCM using 0.1 M [Bu_4N][PF_6] supporting electrolyte, a glassy carbon working electrode, a platinum wire counter electrode, and a Ag wire pseudoreference electrode and internally referenced to the Fc/Fc^+ redox couple. Substrates possessing $E_{1/2}$ > −1.10 V are susceptible to SET from **3b**, leading to FLP reactivity (left), whereas those with $E_{1/2}$ < −1.10 V are unlikely to be reduced and instead directly react with the "hidden" boron radical anion (right). (b) Anisotropic X-band EPR spectrum of **3b** (black) with an overlaid simulation (red) at 100 K revealing a ^{51}V-centered reduction with possible electron delocalization along the V⋯N⋯B framework. (See the SI for simulation parameters.) (c) Spin-density map of **3b** calculated by DFT and revealing a non-negligible contribution on B (13%), suggestive of "hidden" boron radical character.

https://dx.doi.org/10.1021/acs.inorgchem.0c01464
Inorg. Chem. XXXX, XXX, XXX−XXX

resonances attributed to the $[CoCp^*_2]^+$ cation between 0.5 and 2.1 ppm (Figure S53). Upon scaling up the reaction, single crystals suitable for XRD studies were grown, and the solid-state structure unequivocally revealed the formation of the $[CoCp^*_2]^+$ C−H activated product, **4a** (Figure 4). The bond metrics along the V−N−B bonds in **4a** are similar to those found in **1a** (Table S1) and are consistent with the observed oxidation to a diamagnetic V^V center.

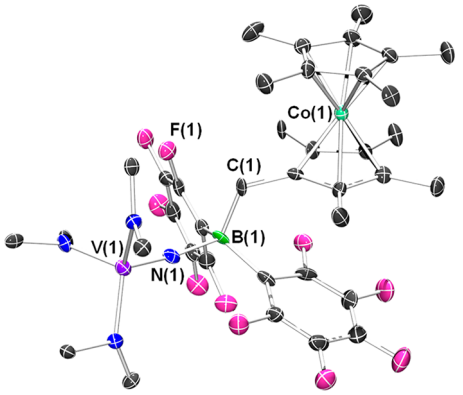

Figure 4. Solid-state molecular structure of **4a**. Phenyl C−H linkages, hydrogen atoms, and cocrystallized solvent molecules are omitted for clarity.

The methyl C−H bond activation of $[CoCp^*_2]^+$ in the conversion of **3a** to **4a** involved the formal loss of H·, the fate of which remains unknown. However, we observed that the addition of the stable phenoxyl radical, 2,4,6-tBu$_3$C$_6$H$_2$O· (**ArO·**), to **3a** resulted in the clean formation of **4a** and **ArOH**. We also note that compound **3b** does not undergo this spontaneous decomposition but does initiate the $[CoCp^*_2]^+$ C−H activation in the presence of **ArO·**. Taken together, we hypothesized that the C−H bond activation chemistry likely proceeded through one of two mechanisms: (1) via a FRP-induced homolytic C−H cleavage mechanism involving the **ArO·** and "hidden" boron radical anion (**3a,b**) (Scheme 2, left; Figure 3c), reminiscent of previously proposed FRP[44] and boron radical C−H reactivity,[21] or (2) via initial SET from the anion of **3a,b** to **ArO·** to generate the FLP composed of $\mathbf{ArO}^-$ and **1a,b** (Scheme 2, right). Subsequent deprotonation at one of the acidic methyl C−H bonds in $[CoCp^*_2]^+$ would result in the formation of **4a,b**.[52−54] A similar SET from a related borole radical to TEMPO, followed by C−H deprotonation at $[CoCp^*_2]^+$, was recently reported.[20]

Scheme 2[a]

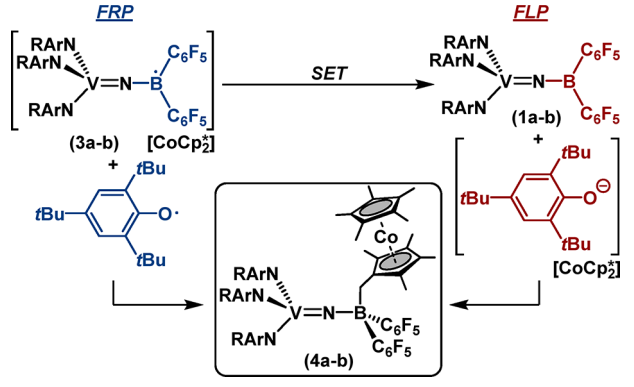

[a]Proposed FRP composed of the boron radicals **3a,b** and **ArO·** performing C−H bond activation of $[\mathbf{CoCp^*_2}]^+$ (left). Alternatively, SET from **3a,b** to **ArO·** would generate an FLP composed of **1a,b** and ArO^-, which could deprotonate the acidic methyl C−H bond in $[\mathbf{CoCp^*_2}]^+$, generating the products **4a,b** (right).

To distinguish between these possible mechanisms, a simple comparison of the $V^{IV/V}$ redox couple in **1/3** relative to the $\mathbf{ArO}^{\bullet/-}$ couple should reveal whether SET is favored. The CV of **ArO·** was taken in DCM and revealed a clean reversible $\mathbf{ArO}^{\bullet/-}$ couple at $E_{1/2}$ = −0.91 V vs Fc/Fc$^+$ (Figure 3a). Whereas the $E_{1/2}$ value of **1a/3a** could not be obtained due to the aforementioned instability of these complexes, the **1b/3b** couple at $E_{1/2}$ = −1.10 V vs Fc/Fc$^+$ (*vide supra*) does support a favorable (ΔG = −19 kJ/mol) SET event (Figure 3a). Thus mechanistically, it is likely that the chemistry proceeded via an FLP-type mechanism involving an initial SET from **3b** to **ArO·** to generate the $\mathbf{1b/ArO}^-$ FLP, which initiated the observed C−H functionalization.[20]

Whereas the combination of **3a,b** with **ArO·** likely generated an intermediate FLP for C−H activation of $[CoCp^*_2]^+$, our DFT studies nonetheless indicated that radical character at boron should also be accessible (Figure 3c). As previously noted, boron radicals are invoked in FRP chemistry and are typically probed by homolytic bond cleavage reactions at peroxides or Sn−hydrides.[19−23] To discount possible initial SET to any of these reagents, we first collected the CV data of both dibenzoyl peroxide (PhC(O)OOC(O)Ph) and Ph_3SnH. The CV data of (PhC(O)OOC(O)Ph) collected in DCM revealed an irreversible reduction event at E^{red}_{peak} = −1.92 V (Figure 3a). Similarly, an irreversible reduction event was observed for Ph_3SnH near the electrochemical window of acetonitrile (E^{red}_{peak} = −2.74 V, Figure S81). Thus any SET event from **3b** to either of these reagents should be highly unfavorable (ΔG > 85 kJ/mol). Exposing either **3b** or **3b′** (both paramagnetic) to a half-equivalent of PhC(O)OOC(O)Ph in DCM led to the clean emergence of new, diamagnetic, analogous products, as observed by multinuclear NMR spectroscopy. In particular, a sharp resonance in the ^{11}B NMR (−4.2 ppm), with corresponding meta/para-shifted resonances in the ^{19}F NMR spectra (Figures S41−S45), emerged and is consistent with four-coordinate boron centers.[43] A significantly shifted ^{51}V NMR resonance (−311 ppm) also emerged from this reaction. Whereas suitable single crystals for XRD studies were not obtained from the **3b** reaction, they were obtained from the **3b′** reaction, albeit in low resolution, and the solid-state structure confirmed the formation of a new carboxylate B−O product (**5b′**) generated through the homolytic peroxide cleavage expected from boron radical reactivity (Figure 5).[19−23] We note that the reaction with **3a** produced the analogous carboxylate product, **5a** (Figure S77).

Lastly, we explored the reactivity of **3b/3b′** with Ph_3SnH. While again the emergence of diamagnetic products was observed by NMR spectroscopy, including a doublet resonance in the ^{11}B NMR spectrum that collapsed to a singlet in the ^{11}B{^{1}H} spectrum, indicating a B−H bond, we were unable to obtain a clean product in this case (Figures S57−S61). However, the analysis of the ^{119}Sn NMR spectrum revealed the formation of a single new product with a chemical shift at −142.4 ppm (Figure S60), similar to those reported for $Ph_3SnSnPh_3$ in various solvents.[12] Upon working up the crude reaction mixture, this product was isolated and unambiguously

https://dx.doi.org/10.1021/acs.inorgchem.0c01464
Inorg. Chem. XXXX, XXX, XXX−XXX

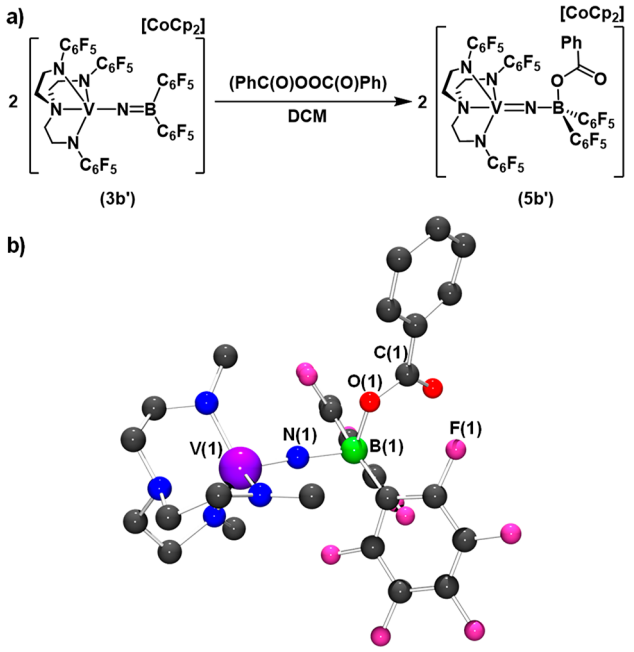

Figure 5. (a) Reaction of **3b′** with PhC(O)OOC(O)Ph led to homolytic peroxide cleavage and B−O carboxylate bond formation (**5b′**), indicative of boron radical reactivity. (b) Low-resolution isotropic solid-state molecular structure of **5b′**. C_6F_5 groups on tren (except for ipso carbons), $[CoCp_2]^+$, hydrogen atoms, and cocrystallized solvent molecules are omitted for clarity.

identified by XRD studies because its unit-cell parameters matched the reported values.[55] The formation of this Sn−Sn product is strongly indicative of boron radical reactivity and homolytic bond cleavage, analogous to reported FRP reactivity.[19−23]

CONCLUSIONS

In summary, we have outlined the synthesis of new Lewis-acidic boranes tethered to redox-active vanadium centers. Redox control of the $V^{IV/V}$ pair allowed for controlled borane or boron radical anion reactivity mimicking FLP or FRP reactivity, respectively. We are further investigating the potential use of such main-group/metal platforms for new cooperative small-molecule or bond-activation chemistry.

EXPERIMENTAL SECTION

General Considerations. All manipulations were performed under an atmosphere of dry, oxygen-free N_2 or Ar through standard Schlenk or glovebox techniques (MBraun UNIlab Pro SP Eco equipped with a −38 °C freezer). Pentane, diethyl ether, benzene, toluene, THF, and DCM were dried using an Mbraun solvent purification system. 2,2,4-Trimethylpentane (iso-octane), hexamethyldisiloxane (HMDSO), acetonitrile, acetonitrile-d_3, benzene-d_6, chloroform-d, dichloromethane-d_2, and tetrahydrofuran-d_8 were purchased from Aldrich or Cambridge Isotope Laboratories, degassed by freeze−pump−thaw, and stored on activated 4 Å molecular sieves prior to use. Ph_2NH, ^{n}BuLi (1.6 M in hexanes), $VCl_3(THF)_3$, Me_3SiN_3, $^i Pr_2NH$, and (PhC(O)OOC(O)Ph) were purchased from Aldrich, Strem, or other commercial vendors and used as received. $Co(C_5Me_5)_2$ and $Co(C_5H_5)_2$ were purchased from Aldrich and sublimed prior to use. $(C_6F_5)_2BCl$,[29] $(Ph_2N)_3V(\mu\text{-}N)Li(THF)_3$,[30] 2,4,6-$^t Bu_3C_6H_2O^{\cdot}$,[56] $N(CH_2CH_2NH(C_6F_5))_3$,[31] $V(NTMS_2)_3$,[32] and $^i PrNHLi$[30] were prepared according to literature procedure. Elemental analyses (C, N, H) were performed at the University of California, Berkeley using a PerkinElmer 2400 Series II combustion analyzer.

Spectroscopic Analyses. NMR spectra were obtained on a Varian Unity Inova 600 MHz, Varian Unity Inova 500 MHz, or Agilent Technologies 400 MHz spectrometer and referenced to the residual solvent of acetonitrile-d_3 (1.94 ppm), benzene-d_6 (7.16 ppm), D_2O (4.79 ppm), dichloromethane-d_2 (5.32 ppm), methanol-d_4 (3.31 ppm), or tetrahydrofuran-d_8 (1.73 ppm) or externally (^{11}B: $BF_3{\cdot}Et_2O$; ^{19}F: $CFCl_3$; ^{51}V: $VOCl_3$; ^{31}P: 85% H_3PO_4; ^{119}Sn: Me_4Sn; ^{7}Li: 9.7 M LiCl in D_2O). Chemical shifts (δ) are recorded in ppm, and the coupling constants are in hertz. X-band EPR spectra were collected on a Bruker EMX EPR spectrometer equipped with an Oxford ESR 900 liquid-helium cryostat. A modulation frequency of 100 kHz was used for all EPR spectra, and the data were plotted using Origin. EPR simulations used the program QPOWA by Belford and coworkers, as modified by J. Telser.[57]

X-ray Crystallography. Data were collected on a Bruker KAPPA APEX II diffractometer equipped with an APEX II charge-coupled device (CCD) detector using a TRIUMPH monochromator with a Mo Kα X-ray source (α = 0.71073 Å). The crystals were mounted on a cryoloop with Paratone-N oil, and all data were collected at 100(2) K using an Oxford nitrogen gas cryostream system. A hemisphere of data was collected using ω scans with 0.5° frame widths. Data collection and cell parameter determination were conducted using the SMART program. Integration of the data frames and final cell parameter refinement were performed using SAINT software. Absorption correction of the data was carried out using SADABS. Structure determination was done using direct or Patterson methods and difference Fourier techniques. All hydrogen atom positions were idealized and rode on the atom of attachment. The structure solution, refinement, graphics, and the creation of publication materials were performed using SHELXTL or OLEX.[2] All POV-Ray depictions of the solid-state molecular structures are shown at the 50% probability ellipsoid level unless otherwise noted.

Electrochemical Analyses. CV was performed on a CH Instruments 630E electrochemical analysis potentiostat, equipped with a 3 mm diameter glassy carbon working electrode, a Ag wire pseudoreference electrode, and a Pt counter electrode with $[Bu_4N][PF_6]$ (0.1 M) supporting electrolyte solution in CH_2Cl_2 or CH_3CN. The glassy carbon working electrode was cleaned prior to each experiment by polishing with 1, 0.3, and 0.05 mm alumina (CH Instruments) in descending order, followed by sonication in distilled water for 2 min. All voltammograms were referenced to the Fc/Fc^+ redox couple.

Density Functional Theory Calculations. DFT calculations were performed using ORCA 4.[58] The geometry optimization of the anion of **3b** was carried out using the UKS TPSS0 method with the def2-TZVP basis set[59−61] and with the relativistic effect, which was accounted for by the zero-order regular approximation (ZORA),[62−64] implemented in the ORCA software. The electric and magnetic hyperfine structure was calculated for B and V centers only.

Synthesis of $(Ph_2N)_3V(\mu\text{-}N)B(C_6F_5)_2$ (1a). To a cold (−35 °C) solid mixture of $ClB(C_6F_5)_2$ (0.190 g, 0.5 mmol) and $(Ph_2N)_3V(\mu\text{-}N)Li(THF)_3$ (0.414 g, 0.5 mmol) was added cold ether (10 mL, −35 °C). The reaction stood at −35 °C for 2 days with intermittent stirring for 1 min every 12 h. The mixture was filtered; then, the solvent was removed in vacuo. The residue was washed with cold pentane (4 × 5 mL), and the solid was dried in vacuo for 20 min to afford a dark-brown solid (0.310 g, 0.34 mmol, 68% yield). Single crystals suitable for XRD studies were obtained by cooling a concentrated toluene/pentane solution of **1a** to −35 °C and standing overnight. ^{1}H NMR (400 MHz, C_6D_6, 25 °C): δ = 6.91−6.85 (m, 24H; Ar*H*), 6.71 (m, 6H; Ar*H*). A small amount of THF and ether (~0.5 equiv total) in the product could not be removed in vacuo, which may due to the Lewis acidity of **1a**. ^{13}C NMR (100 MHz, C_6D_6, 25 °C): δ = 154.4, 128.9, 125.5, 123.2 (*Ph*$_2$N). The signal-to-noise ratio was too low to properly identify any C_6F_5 ^{13}C resonances. ^{51}V NMR (105 MHz, C_6D_6, 25 °C): δ = 119.6 (br). ^{13}B NMR (128 MHz, C_6D_6, 25 °C): δ = 31.8 (br). ^{19}F NMR (376 MHz, C_6D_6, 25 °C): δ = −131.0 (m, 4F; *o*-C_6F_5), −151.7 (t, J = 18.8 Hz, 2F; *p*-C_6F_5), −162.1 (m, 4F; *m*-C_6F_5). Elemental analysis (%) calc. for $C_{48}H_{30}BF_{10}N_4V$ (**1a**) (914.5315 g·mol^{-1}): C, 63.04; H, 3.31; N,

https://dx.doi.org/10.1021/acs.inorgchem.0c01464
Inorg. Chem. XXXX, XXX, XXX−XXX

6.13. Found: C, 60.14; H, 3.30; N, 6.06. Attempts to obtain satisfactory elemental analysis consistently resulted in reduced carbon percentages, likely due to incomplete combustion.[65]

Synthesis of $(N(CH_2CH_2N(C_6F_5))_3)V(\mu\text{-}N)B(C_6F_5)_2$ (1b). *Part 1: Synthesis of ((tren)VNTMS).* To a solution of $N(CH_2CH_2NH(C_6F_5))_3$ (0.545 g, 0.846 mmol) in THF (3 mL) was added $V(NTMS_2)_3$ (0.450 g, 0.846 mmol) in THF (5 mL). The purple mixture was sealed in a heavy-walled reaction flask and heated to 70 °C for 3 h until a dark-green solution formed. Under a nitrogen atmosphere, TMS-N_3 (1.1 equiv) was added, and the resulting mixture was resealed and stirred for 5 h at 70 °C to yield a yellow-orange solution. The volatiles were removed in vacuo and washed with pentane until the filtrate became nearly colorless. The filter-cake was then washed with ether (3 × 1 mL) to give a bright-yellow powder (0.659 g, 0.705 mmol, 83.3% yield). Bright-yellow single crystals suitable for XRD studies were grown by vapor diffusion of HMDSO into a saturated ether solution of the product. NMR data: ^{1}H NMR (400 MHz, C_6D_6, 25 °C): δ = 3.30 (t, $^3J_{HH}$ = 8.0 Hz, 6H; CH_2), 2.13 (t, $^3J_{HH}$ = 8.0 Hz, 6H; CH_2), −0.77 (s, 9H; CH_3). ^{13}C NMR (100 MHz, C_6D_6, 25 °C): δ = 57.8 (CH_2), 53.3 (CH_2), −1.8 (CH_3). The signal-to-noise ratio was too low to properly identify any C_6F_5 ^{13}C resonances. ^{51}V NMR (105 MHz, C_6D_6, 25 °C): δ = −259.3 (br). ^{19}F NMR (376 MHz, C_6D_6, 25 °C): δ = −149.2 (d, J = 18.5 Hz, 6F; o-C_6F_5), −165.6 (m, 6F; m-C_6F_5), −166.1 (t, J = 21.5 Hz, 3F; p-C_6F_5). Elemental analysis (%) calc. for $C_{27}H_{21}F_{15}N_5SiV$ (779.5025 g·mol^{-1}): C, 41.60; H, 2.72; N, 8.98. Found: C, 41.92; H, 2.69; N, 8.92.

Part 2: Synthesis of ((tren)VNLi(THF)$_3$). To a cooled, stirring solution of ((tren)VNTMS) (1.0 g, 1.28 mmol) in THF (4 mL) was added ^{i}PrNHLi (0.117 g, 1.79 mmol) as a suspension in pentane (3 mL) to induce an immediate darkening of the solution to yellow-green. The reaction was monitored by ^{19}F NMR, and (if needed) additional aliquots of ^{i}PrNHLi reagent were added to ensure the complete consumption of the starting material. The reaction was stirred for 30 min before the volatiles were removed in vacuo. The residue was washed with pentane (10 × 2 mL) to give a dark microcrystalline powder (0.850 g, 0.912 mmol, 71.3% yield). Single crystals suitable for XRD studies were grown by the slow vapor diffusion of pentane into a saturated solution of the product in THF. NMR data: ^{1}H NMR (400 MHz, C_6D_6, 25 °C): δ = 3.49 (t, $^3J_{HH}$ = 8.0 Hz, 6H; tren CH_2), 2.99 (t, $^3J_{HH}$ = 8.0 Hz, 12H; THF CH_2), 2.17 (t, 6H; $^3J_{HH}$ = 8.0 Hz, 6H; tren CH_2), 1.32 (m, 12H; THF CH_2). ^{13}C NMR (100 MHz, C_6D_6, 25 °C): δ = 67.6 (THF CH_2), 55.7 (tren CH_2), 53.0 (tren CH_2), 25.4 (THF CH_2). The signal-to-noise ratio was too low to properly identify any C_6F_5 ^{13}C resonances. ^{51}V NMR (105 MHz, C_6D_6, 25 °C): δ = −143.1 (br). ^{19}F NMR (376 MHz, C_6D_6, 25 °C): δ = −149.9 (d, J = 22.5 Hz, 6F; o-C_6F_5), −168.7 (t, J = 21.1 Hz 6F; m-C_6F_5), −173.7 (t, J = 22.3 Hz, 6F; p-C_6F_5). Elemental analysis (%) calc. for $C_{36}H_{36}F_{15}LiN_5O_3V$ (929.5735 g·mol^{-1}): C, 46.52; H, 3.90; N, 7.53. Found: C, 46.25; H, 3.98; N, 7.57.

Part 3: Synthesis of ***1b****.* To a stirring solution of ((tren)VNLi(THF)$_3$) (1.0 g, 1.076 mmol) in benzene was added $(C_6F_5)_2BCl$ (0.409 g, 1.076 mmol) in ether/benzene to give a dark-green solution that was stirred for 2 h. The volatiles were removed in vacuo, and the green oily residue was dissolved in DCM and filtered through a Celite plug to remove LiCl. The dark-green residue was minimally dissolved in benzene and then treated with acetonitrile (0.1 mL) to give a yellow precipitate that was collected and washed with pentane (10 × 1 mL) and ether (5 × 1 mL). Upon dissolution into a 1:1 benzene/THF mixture and the removal of all volatiles, an analytically pure dark-green powder was isolated (0.755 g, 0.719 mmol, 66.8% yield). Single crystals suitable for XRD studies were obtained by slow vapor diffusion of HMDSO into a saturated solution of the product in ether. NMR data: ^{1}H NMR (400 MHz, C_6D_6, 25 °C): δ = 3.30 (t, $^3J_{HH}$ = 5.4 Hz, 6H; CH_2), 2.35 (t, $^3J_{HH}$ = 5.4 Hz, 6H; CH_2). ^{13}C NMR (100 MHz, C_6D_6, 25 °C): δ = 60.6 (CH_2), 53.1 (CH_2). The signal-to-noise ratio was too low to properly identify any C_6F_5 ^{13}C resonances. ^{51}V NMR (105 MHz, C_6D_6, 25 °C): δ = −78.9 (br). ^{13}B NMR (128 MHz, C_6D_6, 25 °C): δ = 30.1 (br). ^{19}F NMR (376 MHz, C_6D_6, 25 °C): δ = −133.1 (br, 4F; B o-C_6F_5), −148.4 (br, 6F; tren o-C_6F_5), −149.5 (br, 2F; B p-C_6F_5), −161.4 (br, 4F; B m-C_6F_5), −162.9 (br, 3F; tren p-C_6F_5), −164.9 (br, 6F; tren o-C_6F_5). Elemental analysis (%) calc. for $C_{36}H_{12}BF_{25}N_5V$ (1051.2386 g·mol^{-1}): C, 41.13; H, 1.15; N, 6.66. Found: C, 41.27; H, 1.38; N, 6.67.

Synthesis of 2-F_4. To a stirring solution of **1b** (0.010 g, 0.0095 mmol) and $PMes_3$ (0.00369 g, 0.0095 mmol) in DCM (3 mL) was added tetrafluoro-1,4-benzoquinone (0.00171 g, 0.0095 mmol) in DCM (1 mL) to give an orange solution within minutes. The reaction was stirred for 10 min before the volatiles were removed in vacuo. The residue was washed with pentane (3 × 1 mL) and ether (1 mL) to give a yellow powder (0.011 g, 0.0068 mmol, 71.4% yield). Single crystals suitable for XRD studies were grown by the slow vapor diffusion of pentane into a saturated solution of **2-F_4** in DCM. NMR data: ^{1}H NMR (400 MHz, $CDCl_3$, 25 °C): δ = 7.03 (s, 6H; aryl CH), 3.68 (t, 6H; CH_2), 2.98 (t, 6H; CH_2), 2.38 (s, 9H; CH_3), 2.13 (s, 18H; CH_3). ^{13}C NMR (126 MHz, $CDCl_3$, 25 °C): δ = 147.0 (ipso C), 133.2 (m-CH), 119.9 (o-CMe), 119.1 (p-CMe), 59.6 (CH_2), 53.1 (CH_2), 23.3 (o-CH_3), 21.4 (p-CH_3). The signal-to-noise ratio was too low to properly identify any C_6F_5 ^{13}C resonances. ^{51}V NMR (105 MHz, $CDCl_3$, 25 °C): δ = −300.7 (br). ^{13}B NMR (128 MHz, $CDCl_3$, 25 °C): δ = −2.3 (br). ^{31}P NMR (161 MHz, $CDCl_3$, 25 °C): δ = 70.92 (s). ^{19}F NMR (376 MHz, $CDCl_3$, 25 °C): δ = −134.2 (br, 4F; B o-C_6F_5), −148.0 (br, 6F; tren o-C_6F_5), −155.8 (d, 2F; quinone CF), −156.6 (d, 2F; quinone CF), −160.8 (t, 2F; B p-C_6F_5), −166.9 (t, 4F; B m-C_6F_5), −168.1 (d, 6F; tren o-C_6F_5), −168.7 (t, 3F; tren p-C_6F_5). Elemental analysis (%) calc. for $C_{69}H_{45}BF_{29}N_5PV$ (1619.8310 g·mol^{-1}): C, 51.16; H, 2.80; N, 4.32. Found: C, 50.83; H, 2.45; N, 3.96.

Synthesis of 2-H_4. The synthesis of **2-H_4** was carried out in a manner identical to that of **2-F_4**, except benzoquinone was used in place of tetrafluoro-1,4-benzoquinone. The resulting product was characterized crystallographically. Single crystals suitable for XRD studies were grown by the slow vapor diffusion of iso-octane into an ether solution of the product.

Synthesis of $[(Ph_2N)_3V(\mu\text{-}N)B(C_6F_5)_2][Co(C_5Me_5)_2]$ (3a). A solution of $Co(C_5Me_5)_2$ (0.033 g, 0.1 mmol) in THF (2 mL) was added to a solution of complex **1a** (0.091 g, 0.1 mmol) in THF (3 mL). The reaction mixture stood at room temperature for 15 min, and the solvent was removed in vacuo. The residue was washed with cold ether (2 × 3 mL) to afford a brown solid (0.086 g, 0.0687 mmol, 68.7% yield). Single crystals suitable for XRD studies were obtained by the slow vapor diffusion of pentane into a concentrated difluorobenzene solution of **3a** at room temperature. EPR data were collected at 298 K in benzene (Figure S64) and at 100 K in THF (Figure S65). Elemental analysis (%) calc. for $C_{68}H_{60}BCoF_{10}N_4V$ (1243.9247 g·mol^{-1}): C, 65.66; H, 4.86; N, 4.50. Found: C, 64.62; H, 4.76; N, 4.21.

Synthesis of $[N(CH_2CH_2N(C_6F_5))_3V(\mu\text{-}N)B(C_6F_5)_2][Co(C_5Me_5)_2]$ (3b). To a stirring solution of **1b** (0.100 g, 0.0951 mmol) in ether (3 mL) was added $Co(C_5Me_5)_2$ (0.031 g, 0.0951 mmol) in ether (2 mL) to immediately give a dark-red precipitate that was stirred for 15 min. The volatiles were removed in vacuo, and the red powder was washed with pentane (5 × 1 mL) and ether (5 × 1 mL). The brick-red powder was then dried in vacuo (0.105 g, 0.0760 mmol, 79.9% yield). Single crystals suitable for XRD studies were grown by the slow evaporation of a 10:1 ether/DCM mixture of the product. EPR data were collected at 100 K in DCM (Figure S66). Elemental analysis (%) calc. for $C_{56}H_{42}BCoF_{25}N_5V$ (1380.6318 g·mol^{-1}): C, 48.72; H, 3.07; N, 5.07. Found: C, 48.99; H, 2.73; N, 4.91.

Synthesis of $[N(CH_2CH_2N(C_6F_5))_3V(\mu\text{-}N)B(C_6F_5)_2][Co(C_5H_5)_2]$ (3b′). To a stirring solution of **1b** (0.160 g, 0.152 mmol) in ether (4 mL) was added $Co(C_5H_5)_2$ (0.029 g, 0.152 mmol) in ether (2 mL) to immediately give a dark precipitate that was stirred for 30 min. The volatiles were removed in vacuo, and the dark residue was washed with pentane (10 × 1 mL) and ether (5 × 1 mL) until the filtrate wash was nearly colorless. After the removal of the remaining wash solvent, a dark-red powder was isolated (0.137 g, 0.110 mmol, 72.7% yield). Single crystals suitable for XRD studies were grown by the slow vapor diffusion of HMDSO into a saturated DCM solution of the product. EPR data were collected at 100 K in DCM (Figure S67). Elemental analysis (%) calc. for $C_{46}H_{22}BCoF_{25}N_5V$ (1240.3618 g·mol^{-1}): C, 44.54; H, 1.79; N, 5.65. Found: C, 44.36; H, 1.50; N, 5.59.

https://dx.doi.org/10.1021/acs.inorgchem.0c01464
Inorg. Chem. XXXX, XXX, XXX−XXX

Synthesis of 4a. *Method 1.* A solution of **1a** (0.091 g, 0.1 mmol) in fluorobenzene (3 mL) was combined with a solution of $Co(C_5Me_5)_2$ (0.033 g, 0.1 mmol) in fluorobenzene (1 mL), and the mixture stood at room temperature overnight. The volatiles were removed in vacuo to give a dark-brown powder, and the ^1H, ^{19}F, and ^{51}V NMR analysis of this crude product revealed that **4a** was formed (see Method 2) as the major product (>85%) (Figure S55). Because of the similar solubility of **4a** and the minor impurities, multiple attempts to purify it failed.

Method 2. A solution of **3a** (0.240 g, 0.193 mmol) in THF (6 mL) was combined with a solution of 2,4,6-^{t}Bu$_3$C$_6$H$_2$O· (0.0505 g, 0.193 mmol) in THF (2 mL), and the mixture stood at room temperature for 2 h. The volatiles were then removed in vacuo to give a dark-brown solid powder, and the ^1H NMR of this crude product revealed a 1:1 mixture of **4a** and 2,4,6-^{t}Bu$_3$PhOH. The crude powder was washed with pentane (3 × 5 mL) and then with ether (4 × 4 mL) to give a dark-brown solid (0.050 g, 0.04 mmol, 20.7% yield). The isolated yield was low due to the similar solubility of **4a** and the 2,4,6-^{t}Bu$_3$C$_6$H$_2$OH byproduct. Single crystals suitable for XRD studies were obtained by the slow vapor diffusion of pentane into a concentrated difluorobenzene solution of **4a** at room temperature. ^1H NMR (400 MHz, THF-d_8, 25 °C): δ = 7.16 (t, $^3J_{HH}$ = 7.9 Hz, 2H; *m*-Ar*H*), 7.07 (d, $^3J_{HH}$ = 7.9 Hz, 2H; *o*-Ar*H*), 6.90 (t, $^3J_{HH}$ = 7.6 Hz, 10H; *m*-Ar*H*), 6.78 (d, $^3J_{HH}$ = 7.6 Hz, 10H; *o*-Ar*H*), 6.73 (t, $^3J_{HH}$ = 7.2 Hz, 5H; *p*-Ar*H*), 1.98 (s, 2H; BCH_2), 1.52 (s, 15H; C_5Me_5), 1.42 (s, 6H; C*Me*), 1.09 (s, 6H; C*Me*). ^{13}C NMR (100 MHz, THF-d_8, 25 °C): δ = 155.6, 128.6, 128.2, 124.4, 124.1, 122.7, 119.7 (two sets of phenyl resonances are observed and are attributed to $\pi-\pi$ stacking between one C_6H_5 group and one C_6F_5 group, as observed in the solid-state XRD structure), 94.9, 93.7, 93.0, 91.9 (*C*), 8.4, 7.9, 7.4 (C*Me*). The signal-to-noise ratio was too low to properly identify any C_6F_5 and BCH_2 ^{13}C resonances. ^{51}V NMR (105 MHz, THF-d_8, 25 °C): δ = −155.0 (br). ^{13}B NMR (128 MHz, THF-d_8, 25 °C): δ = −2.0 (br). ^{19}F NMR (376 MHz, THF-d_8, 25 °C): δ = −127.1 (m, 4F; *o*-C_6F_5), −164.2 (t, *J* = 18.8 Hz, 2H; *p*-C_6F_5), −167.0 (m, 4F; *m*-C_6F_5). Elemental analysis (%) calc. for $C_{68}H_{59}BCoF_{10}N_4V$ (1242.9167 g·mol^{-1}): C, 65.71; H, 4.78; N, 4.51. Found: C, 65.35; H, 5.10; N, 4.51.

Synthesis of 4b. To a stirring solution of **3b** (0.050 g, 0.0362 mmol) in DCM (2 mL) was added 2,4,6-^{t}Bu$_3$C$_6$H$_2$O· (0.0095 g, 0.0362 mmol) in DCM (1 mL) to induce an immediate color change to yellow. The solution was stirred for 1 h before all volatiles were removed in vacuo. The residue was washed with pentane (10 × 1 mL) to remove the 2,4,6-^{t}Bu$_3$PhOH byproduct and residual 2,4,6-^{t}Bu$_3$PhO·. The remaining solid was then washed with ether (1 mL), and the remaining yellow powder was dried in vacuo (0.031 g, 0.0224 mmol, 62% yield). Single crystals suitable for XRD studies were grown by the slow vapor diffusion of iso-octane into a 1:1 DCM/ether mixture of the product. NMR data: ^1H NMR (400 MHz, CD_2Cl_2, 25 °C): δ = 3.65 (br, 6H; CH_2), 2.88 (br, 6H; CH_2), 1.61 (br, 15H; C_5Me_5) 1.51 (br, 2H; BCH_2) 1.34 (br, 6H; C*Me*) 0.81 (br, 6H; C*Me*). ^{13}C NMR (100 MHz, CD_2Cl_2, 25 °C): δ = 120.7 (C_5Me_5), 93.5 (CMe), 92.8 (CMe), 92.1 (CMe), 61.0 (CH_2), 55.0 (CH_2), 8.4 (BCH_2), 8.1 (C_5Me_5), 8.0 (C*Me*), 7.8 (C*Me*). The signal-to-noise ratio was too low to properly identify any C_6F_5 ^{13}C resonances. ^{51}V NMR (105 MHz, CD_2Cl_2, 25 °C): δ = −235.7 (br). ^{13}B NMR (128 MHz, CD_2Cl_2, 25 °C): δ = −5.5 (br). ^{19}F NMR (376 MHz, CD_2Cl_2, 25 °C): δ = −127.8 (br, 4F; B *o*-C_6F_5), −148.9 (br, 6F; tren *o*-C_6F_5), −162.8 (br, 2F; B *p*-C_6F_5), −167.5 (br, 4F; B *m*-C_6F_5), −167.4 (br, 6F; tren *m*-C_6F_5), −168.6 (br, 3F; tren *p*-C_6F_5). Elemental analysis (%) calc. for $C_{56}H_{41}BCoF_{25}N_5V$ (1379.6238 g·mol^{-1}): C, 48.75; H, 3.00; N, 5.08. Found: C, 48.41; H, 3.12; N, 4.97.

Synthesis of [(Ph$_2$N)$_3$V(μ-N)B(O(O)CPh)(C$_6$F$_5$)$_2$][Co(C$_5$Me$_5$)$_2$] (5a). The radical anion **3a** was generated *in situ* and then reacted with dibenzoyl peroxide. A solution of **1a** (0.091 g, 0.1 mmol) in THF (3 mL) was mixed with a solution of $Co(C_5Me_5)_2$ (0.033 g, 0.1 mmol) in THF (1 mL), and the solution stood at ambient temperature for 5 min. Dibenzoyl peroxide (12.1 mg, 0.05 mmol) in THF (1 mL) was added to the above solution, and the resulting mixture stood at ambient temperature for 3 h. The volatiles were removed in vacuo to give a greasy red mixture, which was washed with ether (3 × 5 mL) to give a red powder (0.075 g, 0.055 mmol, 55% yield).). Single crystals suitable for XRD studies were obtained by the slow vapor diffusion of pentane into a concentrated difluorobenzene solution of **4a** at room temperature. ^1H NMR (400 MHz, THF-d_8, 25 °C): δ = 7.71 (d, $^3J_{HH}$ = 7.2 Hz, 2H; *o*-Ar*H* of PhCOO), 7.27 (t, $^3J_{HH}$ = 7.2 Hz, 1H; *p*-Ar*H* of PhCOO), 7.71 (d, $^3J_{HH}$ = 7.2 Hz, 2H; *m*-Ar*H* of PhCOO), 6.80 (d, $^3J_{HH}$ = 7.2 Hz, 12H; *m*-Ar*H* of Ph_2N), 6.71 (d, $^3J_{HH}$ = 7.2 Hz, 12H; *o*-Ar*H* of Ph_2N), 6.63 (t, $^3J_{HH}$ = 7.2 Hz, 6H; *p*-Ar*H* of Ph_2N), 1.70 (s, 30H; C_5Me_5). ^{13}C NMR (100 MHz, THF-d_8, 25 °C): δ = 166.9 (PhCOO), 155.4 (Ph_2N), 136.4 (*Ph*COO), 131.0 (*Ph*COO), 130.6 (*Ph*COO), 128.4 (Ph_2N), 127.7 (*Ph*COO), 124.7 (Ph_2N), 122.7 (Ph_2N), 95.0 (C_5Me_5), 7.9 (C_5Me_5). The signal-to-noise ratio was too low to properly identify any C_6F_5 ^{13}C resonances. ^{51}V NMR (105 MHz, THF-d_8, 25 °C): δ = −166.4 (br). ^{13}B NMR (128 MHz, THF-d_8, 25 °C): δ = −1.3 (s). ^{19}F NMR (376 MHz, THF-d_8, 25 °C): δ = −132.5 (m, 4F; *o*-C_6F_5), −164.8 (t, *J* = 18.8 Hz, 2F; *p*-C_6F_5), −168.3 (m, 4F; *m*-C_6F_5). Elemental analysis (%) calc. for $C_{75}H_{65}BCoF_{10}N_4O_2V$ (1365.0397 g·mol^{-1}): C, 65.99; H, 4.80; N, 4.10. Found: C, 65.43; H, 4.68; N, 3.79.

Synthesis of [N(CH$_2$CH$_2$N(C$_6$F$_5$))$_3$V(μ-N)B(O(O)CPh)(C$_6$F$_5$)$_2$]-[Co(C$_5$H$_5$)$_2$] (5b′). To a stirring solution of **3b′** (0.040 g, 0.0322 mmol) in DCM (2 mL) was added dibenzoyl peroxide (0.004 g, 0.016 mmol) in DCM (1 mL) to give an immediate lightening of the solution to orange. The mixture was stirred for 15 min; then, all volatiles were removed in vacuo. The resulting yellow-orange powder was washed with pentane (3 × 1 mL) and ether (5 × 0.5 mL), and the volatiles were removed in vacuo (0.032 g, 0.0235 mmol, 73% yield). Single crystals suitable for XRD studies were grown by the slow vapor diffusion of iso-octane into a saturated solution of the product in DCM. NMR data: ^1H NMR (400 MHz, CD_2Cl_2, 25 °C): δ = 7.96 (d, $^3J_{HH}$ = 8 Hz, 2H; *o*-Ar*H* of PhCOO), 7.50 (br, 1H; *p*-Ar*H* of PhCOO), 7.45 (t, $^3J_{HH}$ = 8 Hz, 2H; *m*-Ar*H* of PhCOO) 5.44 (s, 10H; *CH*) 3.69 (br, 6H; CH_2) 3.00 (br, 6H; CH_2). ^{13}C NMR (100 MHz, CD_2Cl_2, 25 °C): δ = 167.7 (PhCOO), 131.4 (*Ph*COO), 130.1 (*Ph*COO), 128.2 (*Ph*COO), 85.1 (C_5H_5), 60.2 (CH_2), 53.7 (CH_2). The signal-to-noise ratio was too low to properly identify any C_6F_5 ^{13}C resonances. ^{51}V NMR (105 MHz, CD_2Cl_2, 25 °C): δ = −310.7 (br). ^{13}B NMR (128 MHz, CD_2Cl_2, 25 °C): δ = −4.2 (br). ^{19}F NMR (376 MHz, CD_2Cl_2, 25 °C): δ = −134.0 (br, 4F; B *o*-C_6F_5), −148.8 (br, 6F; tren *o*-C_6F_5), −162.6 (br, 2F; B *p*-C_6F_5), −168.0 (br, 4F; B *m*-C_6F_5), −168.0 (br, 6F; tren *m*-C_6F_5), −169.0 (br, 3F; tren *p*-C_6F_5). Elemental analysis (%) calc. for $C_{53}H_{27}BCoF_{25}N_5O_2V$ (1361.4768 g·mol^{-1}): C, 46.76; H, 2.00; N, 5.14. Found: C, 46.57; H, 1.93; N, 4.99.

Synthesis of (C$_6$H$_5$)$_2$NB(C$_6$F$_5$)$_2$. Diphenylamine (0.0338 g, 0.2 mmol) in toluene (3 mL) was added to a solution of $B(C_6F_5)_3$ (0.102 g, 0.2 mmol) in toluene (3 mL) to give a pale-yellow solution that was stirred overnight at 110 °C to give a colorless solution. The volatiles (including the C_6F_5H byproduct) were removed in vacuo to give a pale-yellow solid, which was recrystallized in pentane at −35 °C to give a white solid (0.047 g, 0.092 mmol, 46% yield). ^1H NMR (400 MHz, C_6D_6, 25 °C): δ = 6.95 (d, $^3J_{HH}$ = 7.6 Hz, 4H; *o*-Ar*H*), 6.80 (t, $^3J_{HH}$ = 7.2 Hz, 4H; *m*-Ar*H*), 6.74 (t, $^3J_{HH}$ = 6.8 Hz, 2H; *p*-Ar*H*). ^{13}C NMR (100 MHz, C_6D_6, 25 °C): δ = 146.9 (ipso C), 129.3 (*o*-CH), 127.4 (*m*-CH), 126.7 (*p*-CH). The signal-to-noise ratio was too low to properly identify any C_6F_5 ^{13}C resonances. ^{13}B NMR (128 MHz, C_6D_6, 25 °C): δ = 36.7 (br). ^{19}F NMR (376 MHz, C_6D_6, 25 °C): δ = −132.4 (m, 4F; *o*-C_6F_5), −151.2 (t, *J* = 18.8 Hz, 2F; *p*-C_6F_5), −161.5 (m, 4F; *m*-C_6F_5). Elemental analysis (%) calc. for $C_{24}H_{10}BF_{10}N$ (513.1450 g·mol^{-1}): C, 56.18; H, 1.96; N, 2.73. Found: C, 55.92; H, 1.80; N, 2.62.

■ ASSOCIATED CONTENT

Supporting Information

The Supporting Information is available free of charge at https://pubs.acs.org/doi/10.1021/acs.inorgchem.0c01464.

NMR, EPR, XRD, CV, DFT, crystallographic CIF files (PDF)

https://dx.doi.org/10.1021/acs.inorgchem.0c01464
Inorg. Chem. XXXX, XXX, XXX−XXX

Accession Codes

CCDC 1988821−1988833 contain the supplementary crystallographic data for this paper. These data can be obtained free of charge via www.ccdc.cam.ac.uk/data_request/cif, or by emailing data_request@ccdc.cam.ac.uk, or by contacting The Cambridge Crystallographic Data Centre, 12 Union Road, Cambridge CB2 1EZ, UK; fax: +44 1223 336033.

AUTHOR INFORMATION

Corresponding Author

Gabriel Ménard − *Department of Chemistry and Biochemistry, University of California, Santa Barbara, California 93106, United States;* orcid.org/0000-0002-2801-0863; Email: menard@chem.ucsb.edu

Authors

Anthony Wong − *Department of Chemistry and Biochemistry, University of California, Santa Barbara, California 93106, United States;* orcid.org/0000-0001-6918-2437

Jiaxiang Chu − *Department of Chemistry and Biochemistry, University of California, Santa Barbara, California 93106, United States; School of Chemical Science, University of Chinese Academy of Sciences, Beijing 101408, China*

Guang Wu − *Department of Chemistry and Biochemistry, University of California, Santa Barbara, California 93106, United States*

Joshua Telser − *Department of Biological, Chemical, and Physical Sciences, Roosevelt University, Chicago, Illinois 60605, United States;* orcid.org/0000-0003-3307-2556

Roman Dobrovetsky − *School of Chemistry, Raymond and Beverly Sackler Faculty of Exact Sciences, Tel Aviv University, Tel Aviv 69978, Israel*

Complete contact information is available at: https://pubs.acs.org/10.1021/acs.inorgchem.0c01464

Author Contributions

[⊥]A.W. and J.C. contributed equally.

Notes

The authors declare no competing financial interest.

ACKNOWLEDGMENTS

We thank the National Science Foundation (CHE-1900651), the U.S.-Israel Binational Science Foundation (no. 2018221), the ACS Petroleum Research Fund (no. 58693-DNI3), and the University of California, Santa Barbara for financial support.

REFERENCES

(1) Frey, G. D.; Lavallo, V.; Donnadieu, B.; Schoeller, W. W.; Bertrand, G. Facile Splitting of Hydrogen and Ammonia by Nucleophilic Activation at a Single Carbon Center. *Science* **2007**, *316*, 439−441.

(2) Welch, G. C.; Juan, R. R. S.; Masuda, J. D.; Stephan, D. W. Reversible, metal-free hydrogen activation. *Science* **2006**, *314*, 1124−1126.

(3) Power, P. P. Main-group elements as transition metals. *Nature* **2010**, *463*, 171−177.

(4) Légaré, M.-A.; Bélanger-Chabot, G.; Dewhurst, R. D.; Welz, E.; Krummenacher, I.; Engels, B.; Braunschweig, H. Nitrogen fixation and reduction at boron. *Science* **2018**, *359*, 896−900.

(5) Hicks, J.; Vasko, P.; Goicoechea, J. M.; Aldridge, S. Synthesis, structure and reaction chemistry of a nucleophilic aluminyl anion. *Nature* **2018**, *557*, 92−95.

(6) Stephan, D. W. The broadening reach of frustrated Lewis pair chemistry. *Science* **2016**, *354*, 1248.

(7) Stephan, D. W.; Erker, G. Frustrated Lewis Pair Chemistry: Development and Perspectives. *Angew. Chem., Int. Ed.* **2015**, *54*, 6400−6441.

(8) Stephan, D. W. Frustrated Lewis Pairs: From Concept to Catalysis. *Acc. Chem. Res.* **2015**, *48*, 306−316.

(9) Grimme, S.; Kruse, H.; Goerigk, L.; Erker, G. The Mechanism of Dihydrogen Activation by Frustrated Lewis Pairs Revisited. *Angew. Chem., Int. Ed.* **2010**, *49*, 1402−1405.

(10) Rokob, T. A.; Hamza, A.; Stirling, A.; Soós, T.; Pápai, I. Turning Frustration into Bond Activation: A Theoretical Mechanistic Study on Heterolytic Hydrogen Splitting by Frustrated Lewis Pairs. *Angew. Chem., Int. Ed.* **2008**, *47*, 2435−2438.

(11) Bannwarth, C.; Hansen, A.; Grimme, S. The Association of Two "Frustrated" Lewis Pairs by State-of-the-Art Quantum Chemical Methods. *Isr. J. Chem.* **2015**, *55*, 235−242.

(12) Liu, L.; Cao, L. L.; Shao, Y.; Ménard, G.; Stephan, D. W. A Radical Mechanism for Frustrated Lewis Pair Reactivity. *Chem.* **2017**, *3*, 259−267.

(13) Merk, A.; Großekappenberg, H.; Schmidtmann, M.; Luecke, M.-P.; Lorent, C.; Driess, M.; Oestreich, M.; Klare, H. F. T.; Müller, T. Single-Electron Transfer Reactions in Frustrated and Conventional Silylium Ion/Phosphane Lewis Pairs. *Angew. Chem., Int. Ed.* **2018**, *57*, 15267−15271.

(14) Liu, L. L.; Cao, L. L.; Zhu, D.; Zhou, J.; Stephan, D. W. Homolytic cleavage of peroxide bonds via a single electron transfer of a frustrated Lewis pair. *Chem. Commun.* **2018**, *54*, 7431−7434.

(15) Dong, Z.; Cramer, H. H.; Schmidtmann, M.; Paul, L. A.; Siewert, I.; Müller, T. Evidence for a Single Electron Shift in a Lewis Acid−Base Reaction. *J. Am. Chem. Soc.* **2018**, *140*, 15419−15424.

(16) Liu, L. L.; Stephan, D. W. Radicals derived from Lewis acid/base pairs. *Chem. Soc. Rev.* **2019**, *48*, 3454−3463.

(17) Piers, W. E.; Marwitz, A. J. V.; Mercier, L. G. Mechanistic Aspects of Bond Activation with Perfluoroarylboranes. *Inorg. Chem.* **2011**, *50* (24), 12252−12262.

(18) Soltani, Y.; Dasgupta, A.; Gazis, T. A.; Ould, D. M. C.; Richards, E.; Slater, B.; Stefkova, K.; Vladimirov, V. Y.; Wilkins, L. C.; Willcox, D.; Melen, R. L. Radical Reactivity of Frustrated Lewis Pairs with Diaryl Esters. *Cell Rep. Phys. Sci.* **2020**, *1*, 100016.

(19) Braunschweig, H.; Dyakonov, V.; Jimenez-Halla, J. O. C.; Kraft, K.; Krummenacher, I.; Radacki, K.; Sperlich, A.; Wahler, J. An Isolable Radical Anion Based on the Borole Framework. *Angew. Chem., Int. Ed.* **2012**, *51*, 2977−2980.

(20) Bauer, J.; Braunschweig, H.; Hörl, C.; Radacki, K.; Wahler, J. Synthesis of Zwitterionic Cobaltocenium Borate and Borata-alkene Derivatives from a Borole-Radical Anion. *Chem. - Eur. J.* **2013**, *19*, 13396−13401.

(21) Silva Valverde, M. F.; Schweyen, P.; Gisinger, D.; Bannenberg, T.; Freytag, M.; Kleeberg, C.; Tamm, M. N-Heterocyclic Carbene Stabilized Boryl Radicals. *Angew. Chem., Int. Ed.* **2017**, *56*, 1135−1140.

(22) Cao, L. L.; Stephan, D. W. Homolytic Cleavage Reactions of a Neutral Doubly Base Stabilized Diborane(4). *Organometallics* **2017**, *36*, 3163−3170.

(23) Su, Y.; Kinjo, R. Boron-containing radical species. *Coord. Chem. Rev.* **2017**, *352*, 346−378.

(24) Wong, A.; Guevara, K.; Wu, G.; Ménard, G. Unusual C−H Bond Activation and C(sp3)−C(sp3) Bond Formation at an Fe(II) Bis(amide) Carbene Complex. *Organometallics* **2020**, *39*, 116−122.

(25) Carroll, T. G.; Hunt, C.; Garwick, R.; Wu, G.; Dobrovetsky, R.; Ménard, G. An untethered C3v-symmetric triarylphosphine oxide locked by intermolecular hydrogen bonding. *Chem. Commun.* **2019**, *55*, 3761−3764.

(26) Carroll, T. G.; Garwick, R.; Telser, J.; Wu, G.; Ménard, G. Synthesis, Characterization, and Electrochemical Analyses of Vanadocene Tetrametaphosphate and Phosphinate Derivatives. *Organometallics* **2018**, *37*, 848−854.

(27) Carroll, T. G.; Garwick, R.; Wu, G.; Ménard, G. A Mono-, Di-, and Trivanadocene Phosphorus Oxide Series: Synthesis, Magnetism,

and Chemical/Electrochemical Properties. *Inorg. Chem.* **2018**, *57*, 11543−11551.
(28) Chu, J.; Carroll, T. G.; Wu, G.; Telser, J.; Dobrovetsky, R.; Ménard, G. Probing Hydrogen Atom Transfer at a Phosphorus(V) Oxide Bond Using a "Bulky Hydrogen Atom" Surrogate: Analogies to PCET. *J. Am. Chem. Soc.* **2018**, *140*, 15375−15383.
(29) Parks, D. J.; Piers, W. E.; Yap, G. P. A. Synthesis, Properties, and Hydroboration Activity of the Highly Electrophilic Borane Bis(pentafluorophenyl)borane, HB(C6F5)2. *Organometallics* **1998**, *17*, 5492−5503.
(30) Song, J.-I.; Gambarotta, S. Preparation, Characterization, and Reactivity of a Diamagnetic Vanadium Nitride. *Chem. - Eur. J.* **1996**, *2*, 1258−1263.
(31) Kol, M.; Schrock, R. R.; Kempe, R.; Davis, W. M. Synthesis of Molybdenum and Tungsten Complexes That Contain Triamidoamine Ligands of the Type (C6F5NCH2CH2)3N and Activation of Dinitrogen by Molybdenum. *J. Am. Chem. Soc.* **1994**, *116*, 4382−4390.
(32) Wagner, C. L.; Phan, N. A.; Fettinger, J. C.; Berben, L. A.; Power, P. P. New Characterization of V{N(SiMe3)2}3: Reductions of Tris[bis(trimethylsilyl)amido]vanadium(III) and -chromium(III) To Afford the Reduced Metal(II) Anions [M{N(SiMe3)2}3]− (M = V and Cr). *Inorg. Chem.* **2019**, *58*, 6095−6101.
(33) Galsworthy, J. R.; Green, M. L. H.; Clifford Williams, V.; Chernega, A. N. Syntheses and characterization of amino-(pentafluorophenyl)boranes. Crystal structure of [(Me3Si)2NB-(C6F5)2]. *Polyhedron* **1998**, *17*, 119−124.
(34) Bamford, K. L.; Longobardi, L. E.; Liu, L.; Grimme, S.; Stephan, D. W. FLP reduction and hydroboration of phenanthrene o-iminoquinones and α-diimines. *Dalton Trans.* **2017**, *46*, 5308−5319.
(35) Yi, J.; Yang, W.; Sun, W.-H.; Nomura, K.; Hada, M. Vanadium NMR Chemical Shifts of (Imido)vanadium(V) Dichloride Complexes with Imidazolin-2-iminato and Imidazolidin-2-iminato Ligands: Cooperation with Quantum-Chemical Calculations and Multiple Linear Regression Analyses. *J. Phys. Chem. A* **2017**, *121*, 9099−9105.
(36) Danopoulos, A. A.; Redshaw, C.; Vaniche, A.; Wilkinson, G.; Hussain-Bates, B.; Hursthouse, M. B. Organoimido complexes of tungsten. X-ray crystal structures of W(NC6H11)Cl2(PMe3)3, [W(NC6H11)Cl2(PMe3)3]O3SCF3, [W(NC6H11)Cl(PMe3)4]-BPh4, W[NSi(o-MeC6H4)3]Cl2(PMe3)3, W[NB(mes2)]2Cl2-(PMe3)2, {W(NPh)Cl[O2C2(CF3)4]2}Li and WCl4(PMe2Ph)3. *Polyhedron* **1993**, *12*, 1061−1071.
(37) Weber, K.; Korn, K.; Schorm, A.; Kipke, J.; Lemke, M.; Khvorost, A.; Harms, K.; Sundermeyer, J. Recent Advances in the Synthesis of N-Heteroatom Substituted Imido Complexes Containing a Nitrido Bridge [M = N—E] (M = Group 4, 5 and 6 Metal, E = B, Si, Ge, P, S). *Z. Anorg. Allg. Chem.* **2003**, *629*, 744−754.
(38) Thompson, R.; Chen, C.-H.; Pink, M.; Wu, G.; Mindiola, D. J. A Nitrido Salt Reagent of Titanium. *J. Am. Chem. Soc.* **2014**, *136*, 8197−8200.
(39) Stevenson, L. C.; Mellino, S.; Clot, E.; Mountford, P. Reactions of Titanium Hydrazides with Silanes and Boranes: N−N Bond Cleavage and N Atom Functionalization. *J. Am. Chem. Soc.* **2015**, *137*, 10140−10143.
(40) Clough, B. A.; Mellino, S.; Clot, E.; Mountford, P. New Scandium Borylimido Chemistry: Synthesis, Bonding, and Reactivity. *J. Am. Chem. Soc.* **2017**, *139*, 11165−11183.
(41) Clough, B. A.; Mellino, S.; Protchenko, A. V.; Slusarczyk, M.; Stevenson, L. C.; Blake, M. P.; Xie, B.; Clot, E.; Mountford, P. New Titanium Borylimido Compounds: Synthesis, Structure, and Bonding. *Inorg. Chem.* **2017**, *56*, 10794−10814.
(42) Espada, M. F.; Bennaamane, S.; Liao, Q.; Saffon-Merceron, N.; Massou, S.; Clot, E.; Nebra, N.; Fustier-Boutignon, M.; Mézailles, N. Room-Temperature Functionalization of N2 to Borylamine at a Molybdenum Complex. *Angew. Chem., Int. Ed.* **2018**, *57*, 12865−12868.
(43) Piers, W. E. The Chemistry of Perfluoroaryl Boranes. In *Advances in Organometallic Chemistry*; Academic Press: 2005; Vol. *52*, pp 1−76.
(44) Ménard, G.; Hatnean, J. A.; Cowley, H. J.; Lough, A. J.; Rawson, J. M.; Stephan, D. W. C-H Bond Activation by Radical Ion Pairs Derived from R3P/Al(C6F5)3 Frustrated Lewis Pairs and N2O. *J. Am. Chem. Soc.* **2013**, *135*, 6446−6449.
(45) Culcasi, M.; Berchadsky, Y.; Gronchi, G.; Tordo, P. Anodic behavior of crowded triarylphosphines. ESR study of triarylphosphoniumyl radicals, Ar3P(•+). *J. Org. Chem.* **1991**, *56*, 3537−3542.
(46) Connelly, N. G.; Geiger, W. E. Chemical Redox Agents for Organometallic Chemistry. *Chem. Rev.* **1996**, *96*, 877−910.
(47) Agarwal, P.; Piro, N. A.; Meyer, K.; Müller, P.; Cummins, C. C. An Isolable and Monomeric Phosphorus Radical That Is Resonance-Stabilized by the Vanadium(IV/V) Redox Couple. *Angew. Chem., Int. Ed.* **2007**, *46*, 3111−3114.
(48) Cutsail, G. E., III; Stein, B. W.; Subedi, D.; Smith, J. M.; Kirk, M. L.; Hoffman, B. M. EPR, ENDOR, and Electronic Structure Studies of the Jahn−Teller Distortion in an FeV Nitride. *J. Am. Chem. Soc.* **2014**, *136*, 12323−12336.
(49) Wang, L.; Li, J.; Zhang, L.; Fang, Y.; Chen, C.; Zhao, Y.; Song, Y.; Deng, L.; Tan, G.; Wang, X.; Power, P. P. Isolable Borane-Based Diradical and Triradical Fused by a Diamagnetic Transition Metal Ion. *J. Am. Chem. Soc.* **2017**, *139*, 17723−17726.
(50) As described in ref 48, electron-nuclear double resonance (ENDOR) spectroscopy has shown hyperfine coupling to ^{11}B (I = 3/2, 80%) in an S = 1/2 Fe^{V} complex supported by a tris(imidazolyl) phenylborate ligand. However, the coupling was very weak (maximum magnitude ∼1.5 MHz), much too small to affect the EPR spectra. Therefore, EPR spectroscopy may not be sensitive enough to detect significant hyperfine coupling to ^{11}B in compounds **3a** and **3b**/**3b′**.
(51) The spin Hamiltonian parameters obtained from the EPR spectrum of **3b**, namely, the $\boldsymbol{g}$ values and ^{51}V hyperfine coupling constants, were reproduced by DFT calculations. These calculations suggested rhombicity in both $\boldsymbol{g}$ and $\boldsymbol{A}(^{51}\mathrm{V})$ that was not resolvable by X-band EPR spectroscopy. Therefore, for the ease of comparison, we converted the calculated rhombic tensors (see the SI) to axial ones by taking the average of the two closest components. This gives: calculated $\boldsymbol{g}$ = [1.971, 1.971, 1.985] (g_{iso} = 1.976); $\boldsymbol{A}(^{51}\mathrm{V})$ = [−100, −100, −280] MHz (a_{iso} = −160 MHz), to be compared with experimental: $\boldsymbol{g}$ = [1.980, 1.980, 1.962] (g_{iso} = 1.974); $|\boldsymbol{A}(^{51}\mathrm{V})|$ = [80, 80, 315] MHz ($|a_{iso}|$= 160 MHz).
(52) Buchholz, D.; Astruc, D. The First Decaisopropylmetallocene: One-Pot Synthesis of [Rh(C5iPr5)2]PF6 from [Rh(C5Me5)2]PF6 by Formation of 20 Carbon−Carbon Bonds. *Angew. Chem., Int. Ed. Engl.* **1994**, *33*, 1637−1639.
(53) Buchholz, D.; Gloaguen, B.; Fillaut, J.-L.; Cotrait, M.; Astruc, D. Mono- and Bis(pentaisopropylcyclopentadienyl) Cobalt and Rhodium Sandwich Complexes and Other Decabranched Cyclopentadienyl Complexes. *Chem. - Eur. J.* **1995**, *1*, 374−381.
(54) Hartmann, N. J.; Wu, G.; Hayton, T. W. Trapping of an NiII Sulfide by a CoI Fulvene Complex. *Organometallics* **2017**, *36*, 1765−1769.
(55) Preut, H.; Haupt, H.-J.; Huber, F. Die Kristall-und Molekularstruktur des Hexaphenyl-distannans. *Z. Anorg. Allg. Chem.* **1973**, *396*, 81−89.
(56) Manner, V. W.; Markle, T. F.; Freudenthal, J. H.; Roth, J. P.; Mayer, J. M. The first crystal structure of a monomeric phenoxyl radical: 2,4,6-tri-tert-butylphenoxyl radical. *Chem. Commun.* **2008**, 256−258.
(57) Belford, R. L.; Belford, G. G. Eigenfield expansion technique for efficient computation of field-swept fixed-frequency spectra from relaxation master equations. *J. Chem. Phys.* **1973**, *59*, 853−854.
(58) Neese, F. Software update: the ORCA program system, version 4.0. *WIREs Comput. Mol. Sci.* **2018**, *8*, e1327.
(59) Grimme, S. Accurate Calculation of the Heats of Formation for Large Main Group Compounds with Spin-Component Scaled MP2Methods. *J. Phys. Chem. A* **2005**, *109*, 3067−3077.
(60) Quintal, M. M.; Karton, A.; Iron, M. A.; Boese, A. D.; Martin, J. M. L. Benchmark Study of DFT Functionals for Late-Transition-Metal Reactions. *J. Phys. Chem. A* **2006**, *110*, 709−716.

https://dx.doi.org/10.1021/acs.inorgchem.0c01464
Inorg. Chem. XXXX, XXX, XXX−XXX

(61) Weigend, F.; Ahlrichs, R. Balanced basis sets of split valence, triple zeta valence and quadruple zeta valence quality for H to Rn: Design and assessment of accuracy. *Phys. Chem. Chem. Phys.* **2005**, *7*, 3297−3305.
(62) Lenthe, E. v.; Baerends, E. J.; Snijders, J. G. Relativistic regular two-component Hamiltonians. *J. Chem. Phys.* **1993**, *99*, 4597−4610.
(63) Lenthe, E. v.; Baerends, E. J.; Snijders, J. G. Relativistic total energy using regular approximations. *J. Chem. Phys.* **1994**, *101*, 9783−9792.
(64) Wüllen, C. v. Molecular density functional calculations in the regular relativistic approximation: Method, application to coinage metal diatomics, hydrides, fluorides and chlorides, and comparison with first-order relativistic calculations. *J. Chem. Phys.* **1998**, *109*, 392−399.
(65) Worrell, W. L.; Chipman, J. The Free Energies of Formation of the Vanadium, Niobium, and Tantalum Carbides1. *J. Phys. Chem.* **1964**, *68*, 860−866.

https://dx.doi.org/10.1021/acs.inorgchem.0c01464
Inorg. Chem. XXXX, XXX, XXX−XXX